Journal of Power Sources 221 (2013) 70–77

Contents lists available at SciVerse ScienceDirect

Journal of Power Sources

journal homepage: www.elsevier.com/locate/jpowsour

The distribution of relaxation times as basis for generalized time-domain models for Li-ion batteries

Jan Philipp Schmidt*, Philipp Berg, Michael Schönleber, André Weber, Ellen Ivers-Tiffée

Institut für Werkstoffe der Elektrotechnik (IWE), Karlsruhe Institute of Technology, Adenauerring 20b, D-76131 Karlsruhe, Germany

HIGHLIGHTS

- A new method for creating automated parameterized time-domain models is introduced.
- Impedance measurements in a broad frequency range are performed.
- The Distribution of Relaxation Times (DRT) is calculated.
- The model is successfully validated with different current profiles in the time-domain.
- The advantages and limits of this modeling approach are discussed.

ARTICLE INFO

Article history:
Received 16 March 2012
Received in revised form
27 July 2012
Accepted 31 July 2012
Available online 11 August 2012

Keywords:
Lithium-ion battery
Modeling
DRT
Impedance
EIS
Time-domain

ABSTRACT

A novel approach for the development of a model for Li-ion batteries with the potential for application in on-board diagnostic is introduced. This approach is not tied to a particular electrochemistry, and has the advantages of scalability and automatable parameterization as well as feasibility regarding an implementation on microcontrollers. The dynamic behavior of the cell under test, a Li-ion pouch cell with a graphite anode and a blend cathode, is characterized in an extremely broad frequency range from 100 kHz to 17 μHz. The introduced model gives predictions consistent with the experimental data, its accuracy depends on the assumed number of relaxation times respectively model order. Recommendations concerning application are given and limitations of the approach are discussed.

1. Introduction

There are special requirements for automotive application of battery systems. This has led to an increased number of publications covering methods for simulation and modeling of lithium ion batteries. The range of complexity and parameterization effort is very broad. Our approach features the distribution of relaxation times and is thereby bridging the gap between physically based mathematical models and coarse equivalent circuit models. It combines straightforward parameterization and a structure that is readily implementable on microcontrollers with a scalable degree of detail.

The application of models is always associated with constraints, i.e. accuracy, computational complexity, configuration effort or analytical insight [1]. As there is no "correct" model, the goal must be to select the model, which is optimal under given constraints. In system theory models are ranked in order of their degree of physical interpretability: white box, gray box and black box models [2].

White box models are based on physical and electrochemical partial differential equations. They describe transport processes and electrochemical processes, which can be linked. These models are often simulated applying FEM-Tools, whereby spatial resolution is variable. Calculation effort increases from 0D-models over homogenized or particle 1D models [3,4] to homogenized 2D models [5,6] up to 3D models [7]. Material constants for parameterization are either available from literature or obtained from extensive measurements.

Equivalent circuit models, for example, belong to the class of *gray box* models. They are proposed in variable degrees of detail. Physical insight can be gained by using adequate circuit elements, i.e. for electrical conductivity, charge transfer, electrochemical double layer or diffusion [8]. However, ambiguity of equivalent

* Corresponding author. Tel.: +49 721 608 47583; fax: +49 721 608 47492.
E-mail address: jan.schmidt@kit.edu (J.P. Schmidt).

0378-7753/$ – see front matter © 2012 Elsevier B.V. All rights reserved.
http://dx.doi.org/10.1016/j.jpowsour.2012.07.100

circuit models is a problem. Despite correct description of the clamp behavior, physical interpretation of circuit element values can be misleading [9]. In some cases circuit elements are of fractional nature and cannot be simulated directly in time domain. This can be solved by the implementation of a fractional integrator [10–12] or by approximating the system with a sum of RC elements [8,13]. While generally the spatial resolution of electrode processes in equivalent circuit models is lower compared to white box models, still ladder type models can be used to describe porosity [14–17]. A coarse spatial resolution is achieved via segmentation, as proposed in Refs. [18,19]. In general, equivalent circuit models are parameterized by fitting them to a measured electrochemical impedance spectrum [13,17,20–25]. Alternatively, a current or potential profile is used for parameterization [26–30].

Artificial neuronal networks [31–34], fuzzy logic [35] or NARMAX models [36] are rated among *black box models*, which are mostly used for diagnosis. Certainly their parameters do not allow for a physical interpretation, but on the other hand parameterization can be completely automated and no a priori knowledge of the processes in the batteries is needed.

The introduced model combines the advantages concerning physical insight of a gray box model with the fully automatable parameterization of a black box model. It is based on the idea, that the impedance of a capacitive electrochemical system can be interpreted as a continuous distribution of RC elements in the space of relaxation times. This is a very general assumption, which is not tied to a particular electrochemistry: Batteries and even fuel cells have proven to be well described by models based on that approach [37–40]. Its distinctive property, the ability to nicely visualize physical properties of the studied system, is based on the improved separation of physical processes like charge transfer or diffusion in the space of relaxation times [41].

There every process is represented as local maximum in a continuous distribution function. However, one does usually not operate with a continuous distribution function. Rather, a discretization of this function is used, assuming the impedance to consist not of an infinite, but only a finite number of RC elements.

Choosing this number rather small, the physical interpretability of the continuous distribution function can only be preserved by applying a priori knowledge of the time constants of the physical processes, compare Fig. 1b) and c). Without a priori knowledge, the physical interpretability of the model can only be preserved by using a sufficiently large number of evenly distributed RC elements. For the sake of a fully automated parameterization process, in this paper the latter method will be described.

In the following sections (i) scalability and (ii) automatable parameterization will be discussed. After the experimental chapter the model is validated with different current profiles and limitations of the model are discussed.

2. Theory

The method of the distribution of relaxation times has been successfully applied for years for the analysis of impedance spectra of solid oxide fuel cells (SOFC) [41,42] and has recently been applied for the analysis of lithium ion cells [43,44]. Its major benefit is the better separation of processes with different time constants compared to the Nyquist or Bode plot [41]. An impedance spectrum can be written as integral equation, where $g(\tau)$ represents the distribution of relaxation times:

$$Z(\omega) = R_0 + R_{\text{pol}} \int_0^\infty \frac{g(\tau)}{1 + j\omega\tau} \mathrm{d}\tau. \quad (1)$$

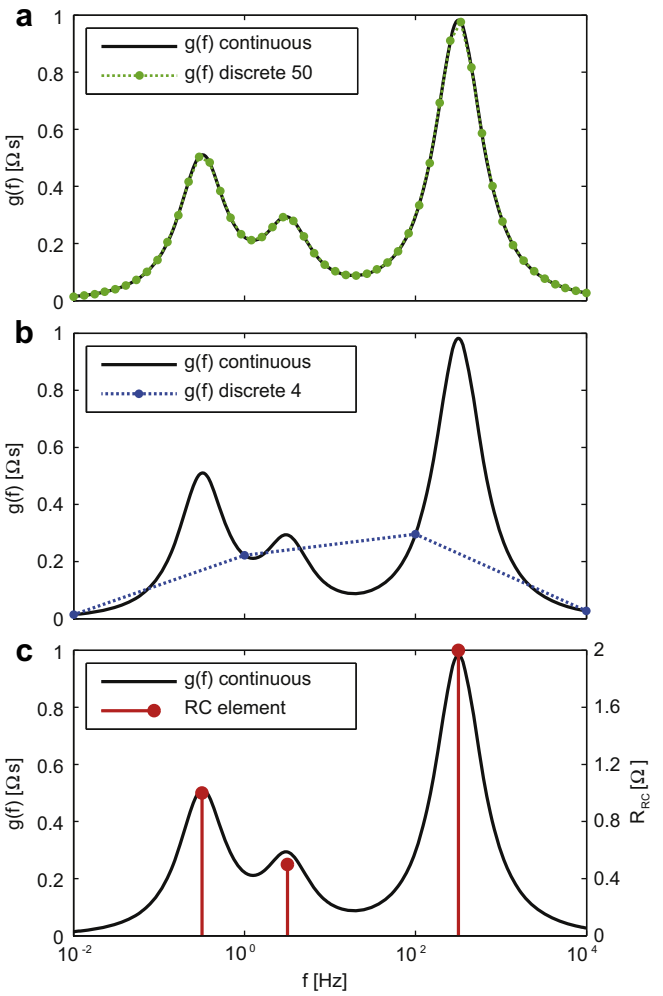

Fig. 1. a) Continuous distribution of relaxation time for an exemplary system exhibiting three different time constants and an approximation with a numerical calculated discrete distribution with an evenly resolution of 50 time constants. b) The continuous distribution in comparison with a discrete distribution comprising only four evenly distributed time constants. c) The continuous distribution function approximated with three RC-elements whose time constants were selected using a priori knowledge.

Since the inversion is performed numerically, the distribution itself is not obtained as an analytical function but as discrete values. Therefore the integral equation becomes a sum:

$$Z(\omega) = R_0 + R_{\text{pol}} \sum_{n=1}^{N} \frac{g_n}{1 + j\omega\tau_n} \delta_{\tau,\log}. \quad (2)$$

Here $\delta_{\tau,\log}$ is the difference between the logarithmically equidistant distributed time constants τ. From this equation it can be deduced, that the measured impedance $Z(\omega)$ can be represented by a serial connection of N RC elements and an ohmic resistance R_0. With an increasing number of relaxation times N, the number of RC elements as well as the computational effort increase.

The according equivalent circuit is depicted in Fig. 2. From equation (2), the calculation of the parameters of the nth RC element can be derived. The resistance of the RC element is calculated as

$$R_n = g_n \cdot \delta_{\tau,\log} \cdot R_{\text{pol}} \quad (3)$$

and the capacitance as

$$C_n = \tau_n / R_n. \quad (4)$$

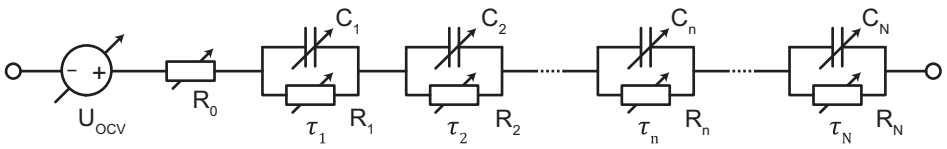

Fig. 2. Introduced equivalent circuit model, based on the distribution of relaxation times and extended for an ohmic resistance and a voltage source for the description of the open circuit voltage.

In this form the model is limited to capacitive systems, whereas purely capacitive and inductive behavior cannot be described. Purely capacitive behavior is observable for frequencies approaching zero. It is caused, for example, by the differential intercalation capacity of battery electrodes [45] and can be modeled by a voltage source (compare Fig. 2) [46], which represents the open circuit voltage (OCV) depending on SOC.

If the measured impedance spectrum shows inductive behavior, a serial inductance or an RL element [47] has to be fitted and subtracted prior to the calculation of the DRT. Afterward this inductance can be added as a serial element to the equivalent circuit model. If the sampling rate of current and voltage is below 100 Hz, inductive behavior cannot be observed. In this case the last step can be omitted.

For implementation the number of relaxation times and the covered frequency range have to be chosen prior to the calculation of the DRT. This allows for easy adjustment of the model regarding complexity, accuracy and calculation effort. Since the time constants are logarithmically equidistantly distributed, each frequency decade is described with the same model order and with the same accuracy. Hence, the dynamic behavior is uniformly modeled for the entire frequency range covered. To demonstrate the straight-forward scalability and the resulting influence on simulation accuracy and speed, models of the order $N = 100, 20, 10$ and 4 are parameterized and compared.

The procedure for parameterization and validation as well as the model structure is summarized in Fig. 3. It contains the following steps:

1) Measurements: (i) C/40 discharge as quasi-stationary OCV-curve, (ii) EIS measurements with a variation of the SOC, (iii) current pulses followed by a relaxation phase with a variation

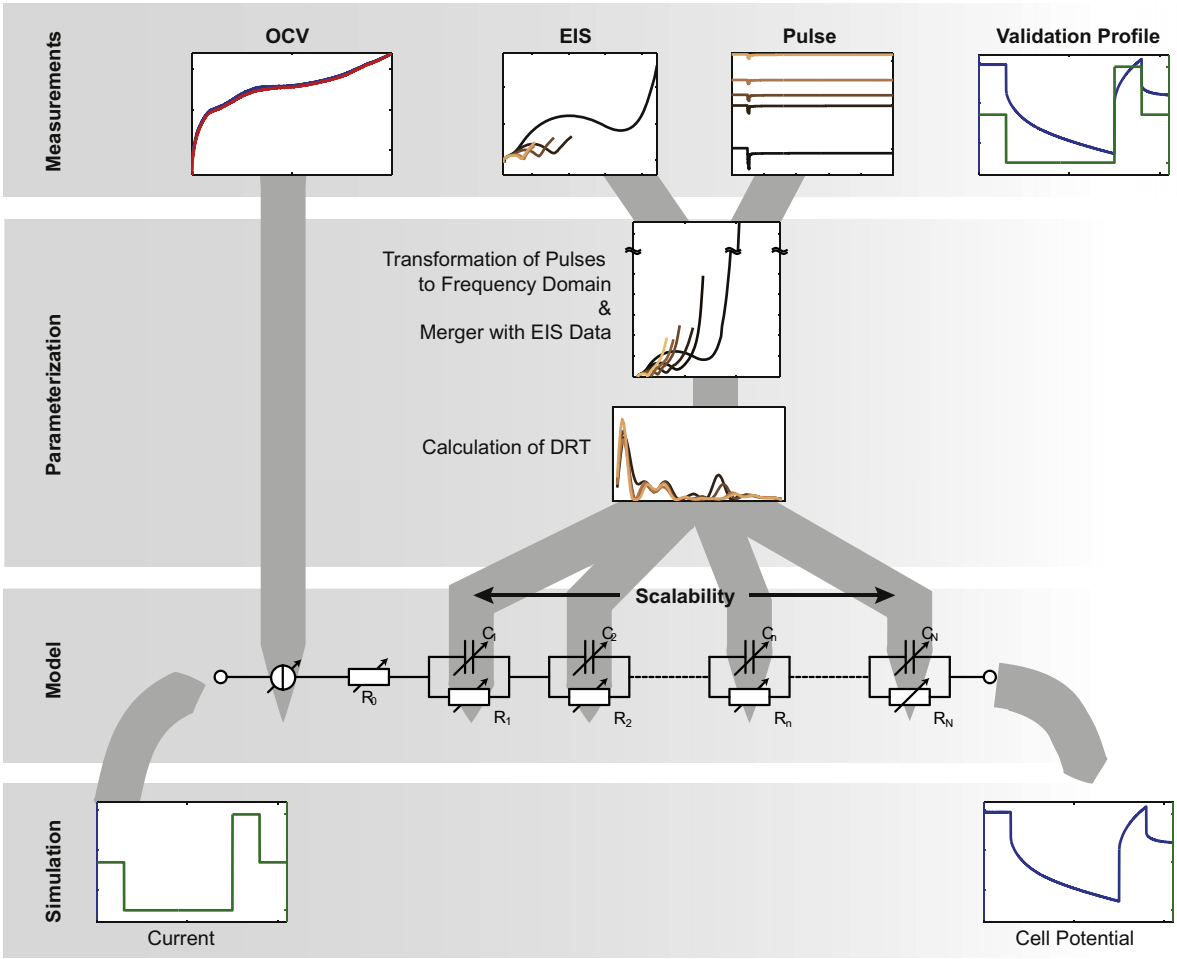

Fig. 3. Flow chart showing the procedure of the parameterization of the DRT-model. The measurement of the validation profile is not necessary for the parameterization but is used for the validation of the model.

of the SOC for parameterization and (iv) current profiles for validation.

2) Parameterization: In order to reduce measurement time, the low frequency part of the impedance spectra is obtained by transforming the current pulse measurements into frequency domain [48]. Then impedance spectra from EIS and pulse measurements are merged and the DRT is calculated for each SOC.
3) Model: The values R_n and C_n obtained from the DRT are used for the parameterization of the RC-model implemented in Matlab/PLECS. The quasi-stationary OCV-curve from step 1) is represented by a controlled voltage source.
4) Simulation and validation: The current profiles applied in step 1) are now simulated and the resulting potential is compared with the measured potential.

All single steps are further explained and discussed in the section Results and discussion.

3. Experimental

The investigated cell is a Li-ion pouch cell from KOKAM (SLPB834374H) with a nominal capacity of 2 Ah. The anode consists of graphite; the cathode is a blend of $LiNi_{0.8}Co_{0.15}Al_{0.05}O_2$/$LiCoO_2$. All measurements were conducted in a climate chamber at 23 °C. The cell was contacted with a clamping device consisting of copper blocks, which realize four-terminal sensing and also serve as heat sinks. All electrochemical experiments were conducted with a 1470E cell test system (Solartron, UK). To increase measurement accuracy for the OCV-curve, the potential was additionally measured with a 34902A data acquisition unit (Agilent, UK).

At the beginning, the actual capacity was measured and the stability of the cell was verified by tenfold repetition of the capacity test. The cell was charged with a current of 1C and then the potential was held at 4.2 V for 1 h. Immediately hereafter, the cell was discharged with a current of 1C until the stop voltage of 2.7 V was reached.

Next the quasi-stationary OCV-curve was recorded: First the cell was charged with the aforementioned charge protocol and then discharged with a current of C/40 until the stop voltage was reached. Then the direction of the current was reversed and the cell was charged with C/40 until the upper stop voltage of 4.2 V was reached. After integration of the current and normalization using the actual capacity from the capacity test, the OCV-curve can be displayed as a function of the SOC, see Fig. 4.

Afterward impedance spectra from an SOC of 95% down to 0% were recorded subsequently in 5% decrements. The potential perturbation amplitude was chosen at 5 mV and the impedance was recorded for frequencies ranging from 100 kHz to 5 mHz with twelve points per frequency decade. After each EIS measurement a relaxation phase of 5 h was inserted, before a current pulse of −2 A with a duration of 10 s was applied. The relaxation of the cell potential was recorded for 40 h. According to the procedure described in Ref. [48], the measurement results from the current pulse measurement have been transformed into frequency domain. The applied algorithm is based on the Fourier transform, allowing the calculation to be performed without prior selection of a model. The impedance spectra from the time-domain measurements are then merged with the impedance spectra from the EIS measurements. Finally the DRT is computed from the merged impedance spectra for a frequency range of 100 kHz down to as low as 17 μHz.

To validate the model in the time domain, after fully charging the cell it was discharged by repeating the current profile shown in Fig. 5. The maximum current I_{max} was varied between C/4 and 4C for different runs, which results in an average discharge current of $I_{max}/2$. In every run, the discharge was stopped as soon as the stop voltage of 2.7 V was reached. This way the dynamic behavior of the cell over the full SOC-range is evaluated.

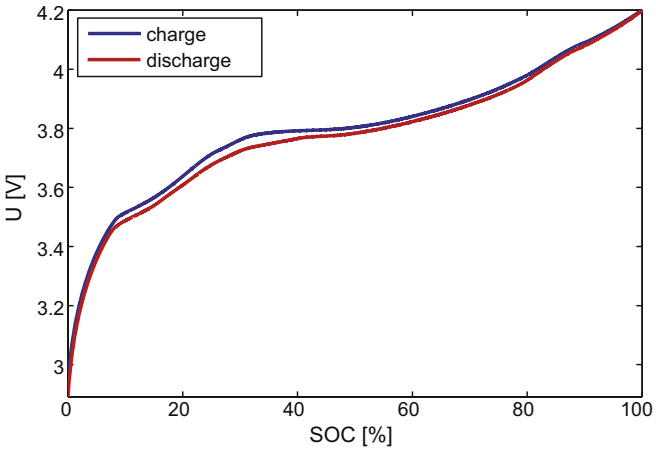

Fig. 4. OCV as function of SOC, measured at constant current discharge and charge with C/40.

4. Results and discussion

4.1. Evaluation of model quality in frequency domain

The merged impedance spectra from EIS and time-domain measurements are depicted in Fig. 6. For a decreasing SOC, the polarization resistance is increasing. The DRT can now be calculated from the obtained impedance data. Prior to the computation the number of time constants has to be selected. For a number of relaxation times $N = 100$ and a frequency range from 3.8 kHz to 17 μHz the resulting DRT is depicted in Fig. 7.

The contributions of the polarization processes are distributed over the whole frequency range. This overall distribution cannot be represented by a standard gray box model like for example two serially connected RC elements. While a dependence on the SOC can hardly be stated for frequencies above 10 Hz, for frequencies between 10 Hz and 1 Hz a distinctive dependence is noticeable. Here the peak frequency decreases monotonously with decreasing SOC and the area beneath the peak increases. This behavior can be attributed to the charge transfer processes, as it was described in a recent publication [49].

The sudden increase of the DRT at low frequencies at an SOC of 0% correlates very well with our observation that relaxation is extremely slow at the end of a complete discharge. However, unlike

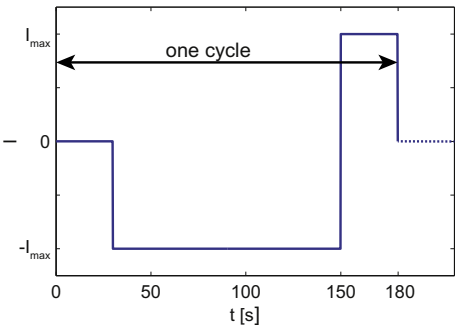

Fig. 5. Single cycle of the current profile for the validation of the model in time domain. The cycles are repeated until the cell potential reaches 2.7 V.

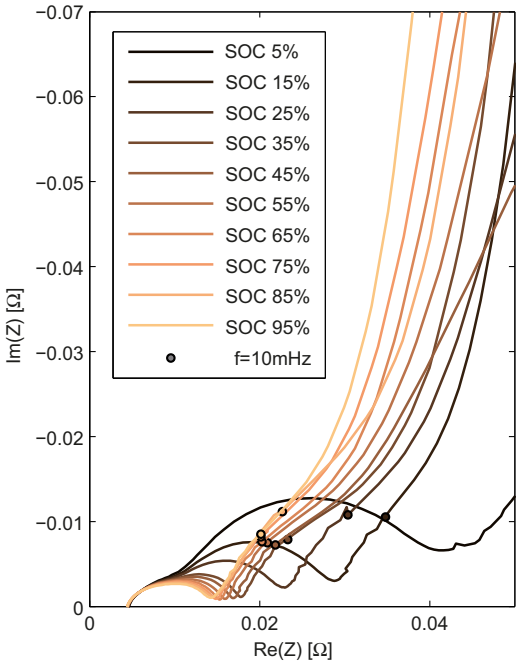

Fig. 6. Measured impedance spectra at different SOCs with frequencies ranging from 100 kHz down to 17 μHz. The frequency range from 100 kHz to 5 mHz was investigated applying EIS measurements, below 10 mHz the impedance was investigated using pulse tests. The overlapping frequency range was used to merge the spectra at 10 mHz (black circles), resulting in one valid impedance spectrum.

the charge transfer process, in the low frequency region a non-monotonous behavior is observed. Although this observation is qualitatively correct, it has to be mentioned that the relaxation phase was not long enough to contain the highest relaxation times, especially for SOCs below 30%. Therefore, some peaks of the lowest frequency process seem to occur at the same lowest observable frequency.

While a physical interpretation is undeniably interesting and the DRT can be applied here with the benefit of separation and identification of processes, this is not necessary for the parameterization of the model. The quality of the parameterized model can be assessed by comparing the measured impedance spectra and the model. Since the impedance of the DRT-model does not contain the differential intercalation capacity, it has to be added for comparison with the measurement data. The very good agreement of measured impedance spectra and calculated spectra from the DRT model is shown in Fig. 8.

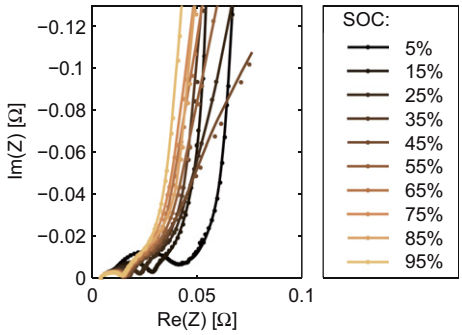

Fig. 8. Measured impedance (points) and impedance of the DRT model with additional differential intercalation capacity (straight line). Measurement and model are in very good agreement.

4.2. Evaluation of model quality in time domain

The simulation result of the validation profile with a number of relaxation times of $N = 100$ is depicted in Fig. 9. A good agreement of simulated and measured battery potential is achieved covering the complete SOC range. For validation profiles with currents up to $I_{max} = 1C$ and SOCs down to 5%, the potential deviation is always lower than 2%. Even though there is a visible drift of the simulated potential over time, short-time dynamics are modeled with high accuracy.

For the profile with a maximum current of 2C the overpotential of the model is consistently too high. This can be explained considering the measured surface temperature of the cell. Since for the validation profile of 2C the surface temperature increases about 5 K (compare Fig. 10), the true impedance of the system is no longer represented by the impedance measured under isothermal conditions. Further, the thermal conductivity of the pouch cell perpendicular to the electrodes is low. Therefore the core temperature of the cell is assumed to be even higher than the measured surface temperature. This higher temperature leads to a decrease of the cell impedance and hence to a decrease of the resulting overpotential. In order to account for this effect a thermal model should be coupled to predict the battery temperature and adapt the modeled impedance.

4.3. Scalability

The aforementioned scalability is given by the freely selectable number of relaxation time constants N. By decreasing N, model complexity and computational effort is decreased. To show the

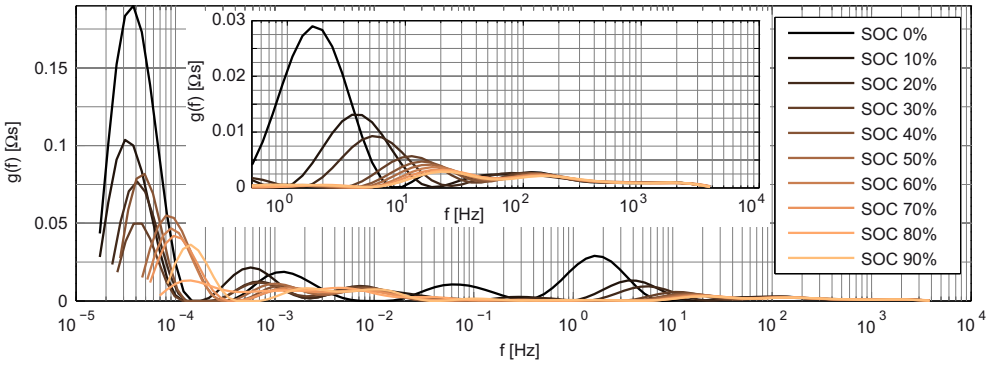

Fig. 7. Distribution of relaxation times for a frequency range from 3.8 kHz to 17 μHz. The SOC is varied from 95% to 5% in 5% decrements. A highly SOC-dependent process can be observed between 1 Hz and 10 Hz. For frequencies higher than 10 Hz, an SOC dependence is not observed, as can be seen from the inset.

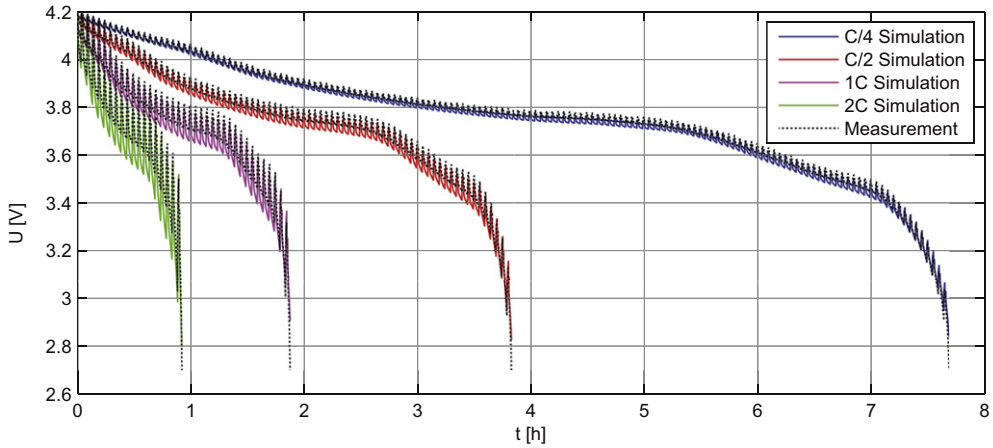

Fig. 9. Validation measurements for current profiles with I_{max} ranging from C/4 to 2C. During the validation profile with I_{max}, the cell is discharged with an average current of $I_{max}/2$. The straight lines show the simulated cell potential, the dotted lines the measured cell potential.

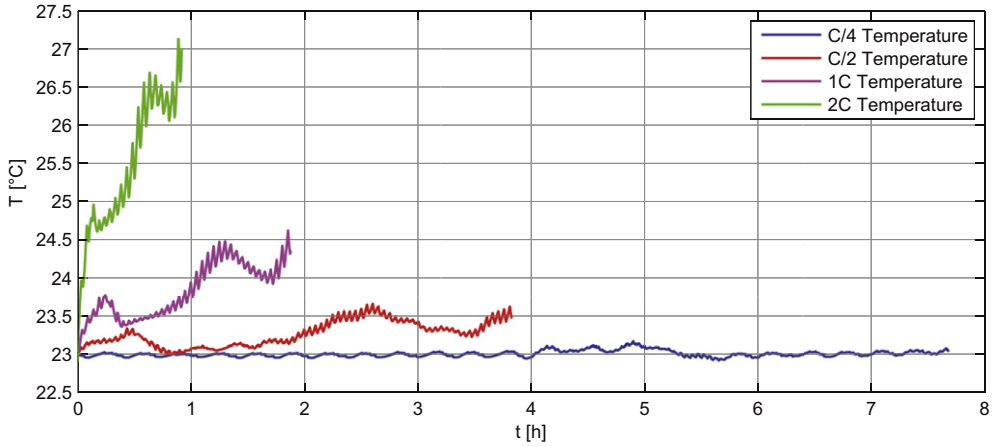

Fig. 10. Measured surface temperature during the validation profiles. For the validation profiles with I_{max} = 1C and 2C maximum current, a significant increase of the surface temperature can be observed.

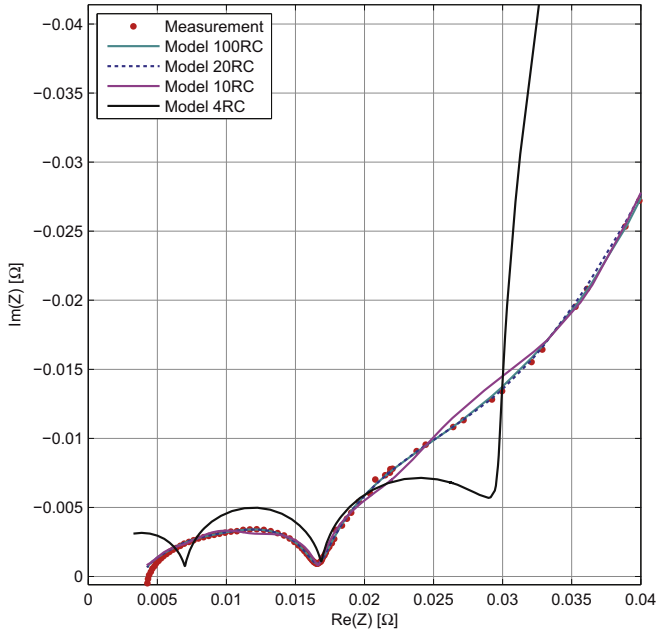

Fig. 11. Measured impedance at an SOC of 50% and impedance of the DRT-models with the orders 100, 20, 10 and 4.

influence of the number of relaxation times on the resulting model impedance, N is varied with N = [100 20 10 4]. The impedance spectra of the models are depicted in Fig. 11. Naturally, with decreasing model order the deviation between measured and modeled impedance increases. For the lowest model order $N = 4$ the semi circles of the RC elements are clearly distinguishable and show a large deviation from the measured impedance. However, already for $N = 20$ the model coincides with the measured impedance very well. Besides the validation in frequency-domain, also validation in time-domain is crucial. As Fig. 12a) shows, on a scale of hours the model quality in time domain does not differ significantly. However, for a timescale of seconds significant differences are observed between the models of order four and ten (compare Fig. 12b)). The model of order four fails to reproduce the measured battery voltage. Among the remaining models of higher order, differences are smaller. Hence it can be concluded, that increasing the model order from $N = 20$ to $N = 100$ does not result in a significantly higher accuracy while the computational effort increases with a factor of five. In sum, the model of order ten is the best tradeoff between accuracy and computational effort and is therefore recommended for the modeled frequency range. Although the absolute number of RC elements seems to be rather high, one has to be aware, that compared to other approaches in literature [22], the covered frequency range is significantly higher.

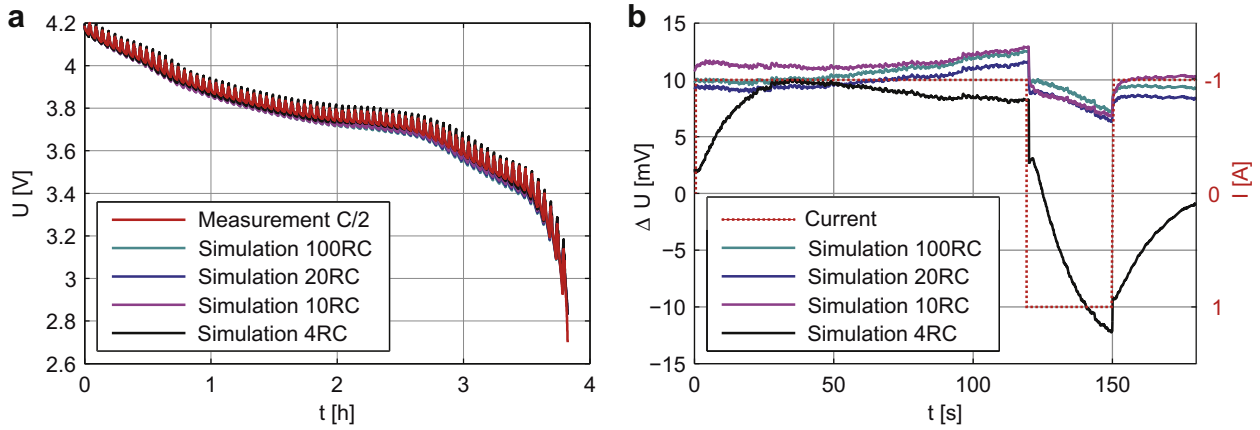

Fig. 12. a) Measured and simulated battery potential for a validation profile with I_{max} = C/2. Model order is varied from 100 down to 4. b) Potential difference between measured and simulated battery potential for only one cycle. The model of order four fails to describe the dynamic cell behavior. A model order of 10 is found to be sufficient.

Table 1
Fraction of real time and simulated time for models of different orders.

Model order, N	100	20	10	4
RC elements/decade	11.6	2.3	1.1	0.5
T_{sim}/T_{real}	9%	0.8%	0.5%	0.3%

Considering the relative number of RC elements per frequency decade, with one RC element per decade, this value is rather low.

An even higher model quality in frequency domain could be achieved by increasing the number of free parameters by not presuming a certain distribution of time constants. This very interesting option was implemented, but due to the increase of computational complexity a full automation of the parameterization processes could not be achieved so far. Finding a solution of this problem will be part of future work.

4.4. Real-time capability

The model order does not only affect accuracy, it also affects the computational effort. Table 1 shows the computation effort as ratio of real time and simulated time T_{real}/T_{sim} together with the number of RC elements per frequency decade for the simulated model orders. All simulations were performed on a desktop computer with an Intel® Core™ i7 CPU using Matlab R2009a (Mathworks) and PLECS 2.1 (plexim). Except for the model of order 100 all simulations could be performed with good real time capability. With respect to the results concerning scalability, the model of order 10 gives the best trade-off for accuracy and computational effort.

5. Conclusion

The introduced model is parameterized using impedance data from a Li-ion pouch cell with a nominal capacity of 2 Ah. It has the potential for application in on-board diagnosis. Because of the generalized approach, the model is independent of material chemistry, microstructure and capacity. Therefore no a priori knowledge of the number and physical origin of the occurring processes is required. Furthermore it combines the advantages of automatable parameterization, scalability and a structure that is directly implementable on microcontrollers. The distribution of relaxation times (DRT), enables (i) a direct derivation of the model from measured impedance data and (ii) a full automation of the parameterization process. Model order and therefore the computational effort are scalable via the discrete number of time constants considered in the model. Also, the considered frequency range can be easily adjusted. Therefore the model is versatile and easily adaptable to various constraints.

As a proof of this concept, the linear behavior of a Li-ion pouch cell was modeled in a wide frequency range. The accuracy in time domain was validated with current profiles, which show that model and measurement are in good agreement up to maximum currents of 1C. Furthermore it was observed that for the investigated high power cell, even currents as low as 1C cause a significant increase of the battery temperature. As this temperature influence is assumed to be responsible for most of the prediction error, coupling of an additional thermal model is expected to be highly beneficial.

Acknowledgments

This work is funded by the Federal Ministry of Education and Research within “Elektrochemie für Elektromobilität – Verbund Süd” (fund number 03KP801) and managed by the Project Management Agency Forschungszentrum Jülich (PTJ). This work was further funded by the “Brennstoffzellen- und Batterie-Allianz Baden-Württemberg”. All responsibility for this publication rests with the authors.

References

[1] R. Rao, S. Vrudhula, D.N. Rakhmatov, Computer 36 (2003) 77–87.
[2] L. Ljung, System Identification: Theory for the User, Prentice Hall, Upper Saddle River, NJ, 1999.
[3] M. Doyle, T.F. Fuller, J. Newman, J. Electrochem. Soc. 140 (1993) 1526–1533.
[4] K. Smith, C.Y. Wang, J. Power Sources 161 (2006) 628–639.
[5] K.H. Kwon, C.B. Shin, T.H. Kang, C.S. Kim, J. Power Sources 163 (2006) 151–157.
[6] U.S. Kim, C.B. Shin, C.S. Kim, J. Power Sources 189 (2009) 841–846.
[7] C.W. Wang, A.M. Sastry, J. Electrochem. Soc. 154 (2007) A1035–A1047.
[8] S. Buller, Impedance-based simulation models for energy storage devices in advanced automotive power systems, In: Aachener Beiträge des ISEA, vol. 31, RWTH Aachen, Aachen, Germany, 2011.
[9] M.E. Orazem, B. Tribollet, Electrochemical Impedance Spectroscopy, John Wiley & Sons, Inc., Hoboken, NJ, 2008.
[10] J. Sabatier, M. Aoun, A. Oustaloup, G. Gregoire, F. Ragot, P. Roy, Signal Process. 86 (2006) 2645–2657.
[11] E. Kuhn, C. Forgez, G. Friedrich, Eur. Phys. J. – Appl. Phys. 25 (2004) 183–190.
[12] A. Benchellal, T. Poinot, J.C. Trigeassou, Signal Process. 86 (2006) 2712–2727.
[13] P.L. Moss, G. Au, E.J. Plichta, J.P. Zheng, J. Electrochem. Soc. 155 (2008) A986–A994.
[14] J.R. Macdonald, Impedance Spectroscopy, John Wiley & Sons, New York, 1987.

[15] R. de Levie, in: , Advances in Electrochemistry and Electrochemical Engineering, vol. 6, 1967, p. 329.
[16] R. de Levie, J. Electroanal. Chem. Interf. Electrochem. 281 (1990) 1–21.
[17] U. Tröltzsch, O. Kanoun, H.R. Tränkler, Electrochim. Acta 51 (2006) 1664–1672.
[18] J.B. Gerschler, F.N. Kirchhoff, H. Witzenhausen, F.E. Hust, D.U. Sauer, in: Vehicle Power and Propulsion Conference, 2009, VPPC '09, IEEE, 2009, pp. 295–303.
[19] M. Fleckenstein, O. Bohlen, M.A. Roscher, B. Bäker, J. Power Sources 196 (2011) 4769–4778.
[20] S. Rodrigues, N. Munichandraiah, A.K. Shukla, J. Solid State Electrochem. 3 (1999) 397–405.
[21] M.J. Isaacson, N.A. Torigoe, R.P. Hollandsworth, in: Battery Conference on Applications and Advances, 1998, The Thirteenth Annual, 1998, pp. 243–246.
[22] D. Andre, M. Meiler, K. Steiner, H. Walz, T. Soczka-Guth, D.U. Sauer, J. Power Sources 196 (2011) 5349–5356.
[23] K. Takeno, M. Ichimura, K. Takano, J. Yamaki, S. Okada, J. Power Sources 128 (2004) 67–75.
[24] M. Dubarry, B.Y. Liaw, J. Power Sources 174 (2007) 856–860.
[25] A. Cuadras, O. Kanoun, in: 6th International Multi-Conference on Systems, Signals and Devices, 2009, SSD '09, 2009, pp. 1–5.
[26] I.S. Kim, J. Power Sources 163 (2006) 584–590.
[27] M. McIntyre, T. Burg, D. Dawson, B. Xian, in: American Control Conference, 2006, 2006, p. 5.
[28] S. Lee, J. Kim, J. Lee, B.H. Cho, J. Power Sources 185 (2008) 1367–1373.
[29] Y. Hu, S. Yurkovich, Y. Guezennec, B.J. Yurkovich, Control Eng. Pract. 17 (2009) 1190–1201.
[30] X. Hu, S. Li, H. Peng, J. Power Sources 198 (2012) 359–367.
[31] P. Jinchun, C. Yaobin, R. Eberhart, in: Battery Conference on Applications and Advances, 2000, The Fifteenth Annual, 2000, pp. 173–177.
[32] M. Ragsdale, J. Brunet, B. Fahimi, in: Vehicle Power and Propulsion Conference, 2008, VPPC '08, IEEE, 2008, pp. 1–6.
[33] Y. Shen, Energy Convers. Manag. 51 (2010) 1093–1098.
[34] A. Affanni, A. Bellini, C. Concari, G. Franceschini, E. Lorenzani, C. Tassoni, in: Electric Machines and Drives Conference, 2003, IEMDC'03, IEEE International, 2003, pp. 684–688.
[35] P. Singh, R. Vinjamuri, X. Wang, D. Reisner, J. Power Sources 162 (2006) 829–836.
[36] G. Guifang, W. Xiaolan, Z. Shiqiong, X. Peng, X. Gang, C. Binggang, in: Vehicle Power and Propulsion Conference, 2008, VPPC '08, IEEE, 2008, pp. 1–4.
[37] H. Sumi, T. Yamaguchi, K. Hamamoto, T. Suzuki, Y. Fujishiro, T. Matsui, K. Eguchi, Electrochim. Acta 67 (2012) 159–165.
[38] A. Leonide, Y. Apel, E. Ivers-Tiffée, ECS Trans. 19 (2009) 81–109.
[39] J. Illig, M. Ender, T. Chrobak, J.P. Schmidt, D. Klotz, E. Ivers-Tiffée, J. Electrochem. Soc. 159 (2012) A952–A960.
[40] C. Graves, S.D. Ebbesen, M. Mogensen, Solid State Ionics 192 (2011) 398–403.
[41] H. Schichlein, A.C. Müller, M. Voigts, A. Krügel, E. Ivers-Tiffée, J. Appl. Electrochem. 32 (2002) 875–882.
[42] A. Leonide, V. Sonn, A. Weber, E. Ivers-Tiffée, J. Electrochem. Soc. 155 (2008) B36–B41.
[43] J.P. Schmidt, T. Chrobak, M. Ender, J. Illig, D. Klotz, E. Ivers-Tiffée, J. Power Sources 196 (2010) 5342–5348.
[44] J. Illig, T. Chrobak, D. Klotz, E. Ivers-Tiffée, ECS Trans. 33 (2011) 3–15.
[45] M.D. Levi, D. Aurbach, J. Phys. Chem. B 101 (1997) 4630–4640.
[46] I. Bloom, A.N. Jansen, D.P. Abraham, J. Knuth, S.A. Jones, V.S. Battaglia, G.L. Henriksen, J. Power Sources 139 (2005) 295–303.
[47] A. Jossen, J. Power Sources 154 (2006) 530–538.
[48] D. Klotz, M. Schönleber, J.P. Schmidt, E. Ivers-Tiffée, Electrochim. Acta 56 (2011) 8763–8769.
[49] D.P. Abraham, S. Kawauchi, D.W. Dees, Electrochim. Acta 53 (2008) 2121–2129.